SUPPORTING INFORMATION:

Directional Photofluidization Lithography for Nanoarchitectures with Controlled Shapes and Sizes

Seungwoo Lee,[†] Jonghwa Shin,[‡] Yong-Hee Lee,[‡§] Shanhui Fan,[▌] and Jung-Ki Park[,†§⊥]*

Department of Chemical and Biomolecular Engineering, Department of Physics, KAIST Institute for the Nanocentury, and KAIST Graduate School of EEWS, Korea Advanced Institute of Science and Technology (KAIST), 335 Gwahangno, Yuseong-gu, Daejeon 305-701, Republic of Korea, and E. L. Ginzton Lab and Department of Electrical Engineering, Stanford University, Stanford, California 94305

*To whom correspondence should be addressed. E-mail: jungpark@kaist.ac.kr. Website: zoo.kaist.ac.kr; web.kaist.ac.kr/~ace51. Tel: +82-42-350-3925. Fax: +82-42-350-3910.

† Department of Chemical and Biomolecular Engineering, KAIST

‡ Department of Physics, KAIST

§ KAIST Institute for the Nanocentury

▌ E. L. Ginzton Lab and Department of Electrical Engineering, Stanford University

⊥ KAIST Graduate School of EEWS

1. Experimental details

Synthesis of azopolymer (polydisperse orange 3): The synthetic procedures of Poly(disperse orange 3) (PDO 3) is available in the literature.[1,2] The weight-average molecular weight and the PDI of PDO 3 were 4700 g/mol and 1.74, respectively. The glass transition temperature (T_g) was 120 °C.

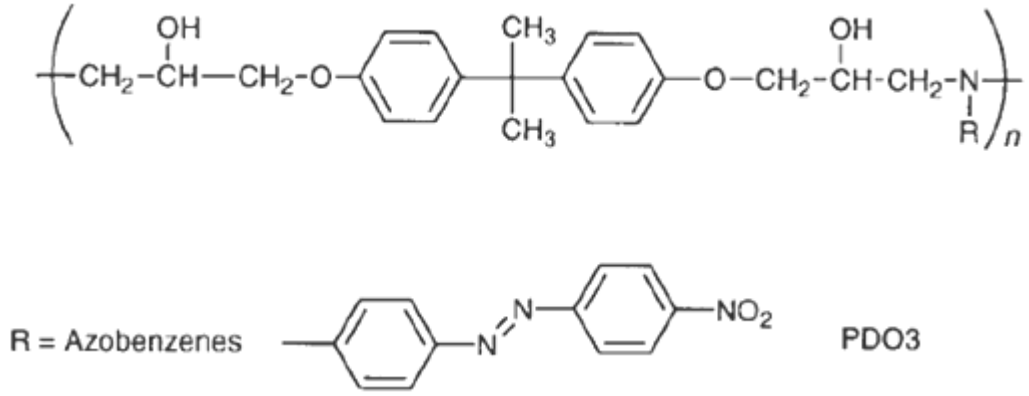

Figure S1. Chemical structures of PDO 3

Preparation of PDMS molds: The master was fabricated by photolithography. In particular, we used standard contact lithography utilizing binary intensity photomasks with line arrays.[3] The height and width of the fabricated gratings were 2.27 μm and 2.47 μm, respectively, and the periodicity of the microgroove was controlled to be 3.84 μm.

To obtain the PDMS mold, a PDMS prepolymer and an initiator (Sylgard 184, Dow Corning, Midland, MI) were mixed at a 10:1 ratio (by weight), and subsequently degassed by vacuum suction. The degassed solution of PDMS was then poured onto a prepared master carefully to prevent the generation of bubbles. Finally, the PDMS solution was cured at 70 ℃ in an oven for 3 h. After it was fully cured, the PDMS mold was released from the master. Figure S2 displays the obtained PDMS mold: the structural features of the PDMS mold including the height, width, and periodicity were comparable to those of the master.

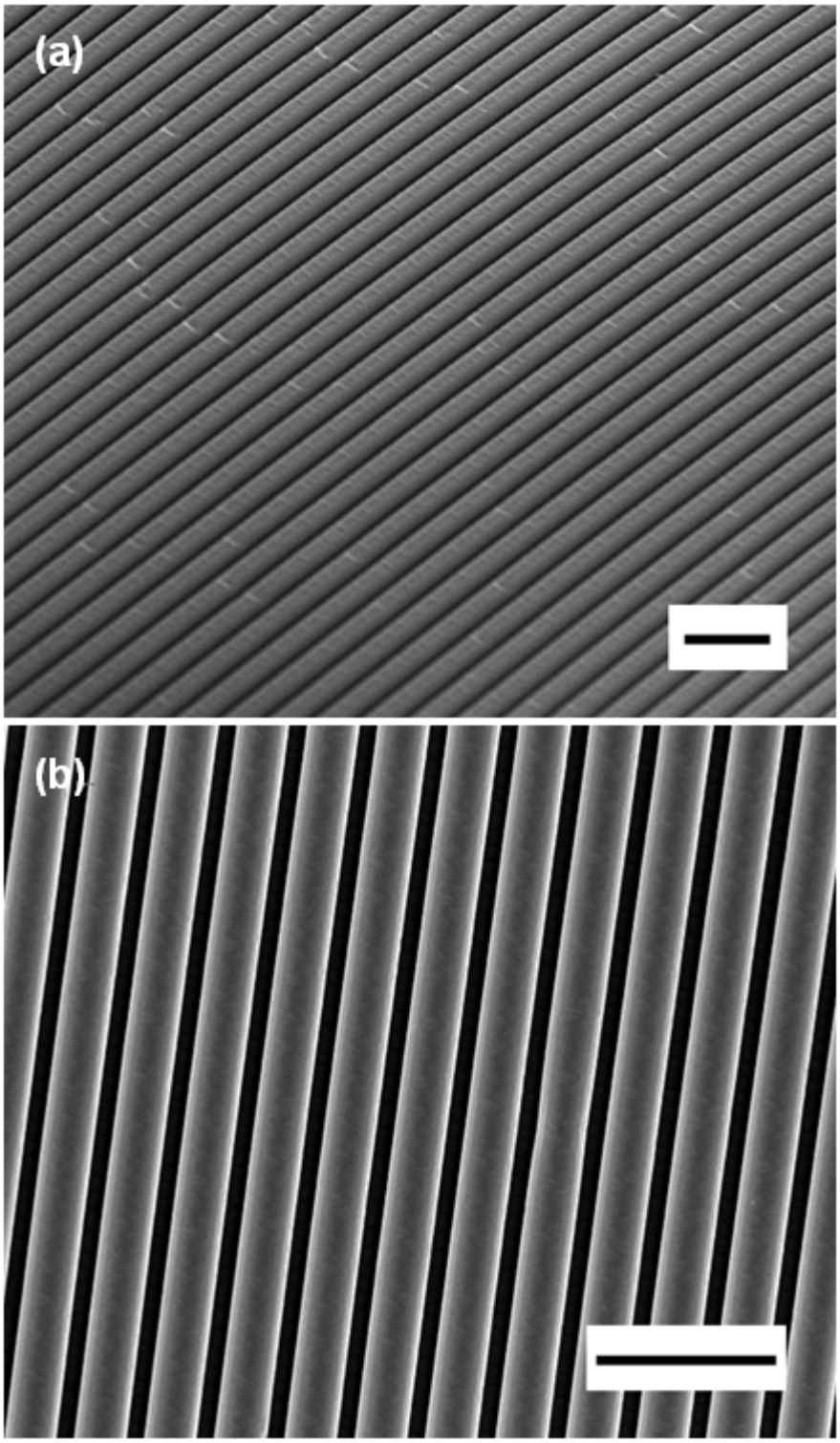

Figure S2. Scanning Electron Microscopy (SEM) images of the PDMS molds used in this study: (a) low-magnification image taken at tilted angle (50 degrees); (b) high-magnification image taken at a normal angle. Scale bars are10 μm.

Micromolding in capillaries (MIMIC) with solvent: The protocols of the MIMIC with solvent were previously established by Whitesides et al.[4,5] Details of the MIMIC process are as follows: The quartz

substrates used here were cleaned by sonication in a 10 wt% sodium hydroxide aqueous solution and deionized water. After drying, the PDMS mold was placed onto a cleaned quartz substrate to form the micro-capillaries. The PDO 3 solution was then dropped into the entrance of the micro-capillaries. Once the capillaries were filled with the PDO 3 solution, the solvent was completely evaporated at room temperature for 3 days. Finally, the PDMS mold was peeled-off from the substrate. PDO 3 line arrays replicating the molds were thus obtained.

Imaging: The structures of the photo-reconfigurable templates and patterned metallic nanostructures (gold nanowire and ellipsoid arrays) were investigated by means of scanning electron microscopy (SEM, FEI, Sirion) and optical microscopy measurements in transmission mode (OM, Olympus, BX51).

2. Optimization of MIMIC with solvent: Effect of the advancing contact angle and the concentration of PDO 3 solution on the imbibition length

A previous report regarding MIMIC suggested that the imbibition and flow of liquids in rectangular capillaries are predominantly defined by the interfacial free energy of the wetting of the capillary or by experimentally observed phenomenon, for example, advancing the contact angle: a high advancing contact angle resulting from low interfacial free energy leads to a high length of capillary imbibition.[5] Therefore, to obtain a high length of capillary imbibition, we used *N*-methyl-2-pyrolidone (NMP) as a solvent due to its low interfacial free energy and resulting high advancing contact angle: although cyclohexanone or cyclopentanone are widely used with PDO 3 solutions, their high interfacial free energy and low advancing contact angle result in a lower length of capillary imbibition compared to that of NMP (see the Supporting Information, Figure S3-4). The concentration of the PDO 3 solution in NMP was controlled to be 1 wt %; a concentration below 1 wt% can lead to a higher length of capillary imbibition than that of 1 wt%, but dewetting and the resulting structural defects are simultaneously generated (see the Supporting Information, Figure S5). The length of capillary imbibition obtained was ~1.8 mm, and structural defects over a large area of PDO 3 line arrays were not observed when using both scanning electron microscopy (SEM) and optical microscopy (OM) (see Figure 1 and Figure S5-6). The low-magnification of OM image clearly shows the moiré fringes due to the uniformly patterned PDO 3 lines over a large area (~ 3.3 mm^2) as shown in Supporting Information, Figure S6; FT of the corresponding OM image further supports the long-range order within PDO 3 line arrays. The width and periodicity of the PDO 3 line arrays obtained were 1.30 μm and 3.84 μm, respectively. The thickness of PDO 3 was 1.30 μm. These values are comparable to those of the PDMS mold.

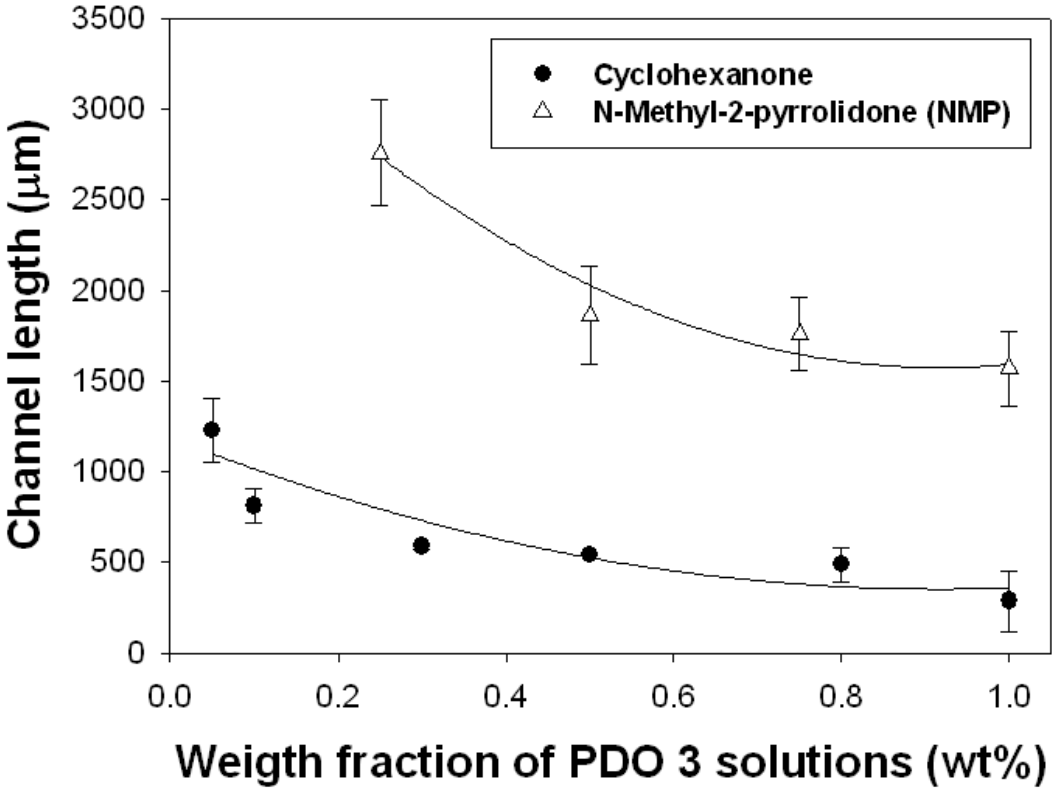

Figure S3. Imbibition length of the PDO 3 lines versus the weight fraction of the PDO 3 solution: NMP with low interfacial free energy led to a much higher imbibition length than cyclohexanone with high interfacial free energy.

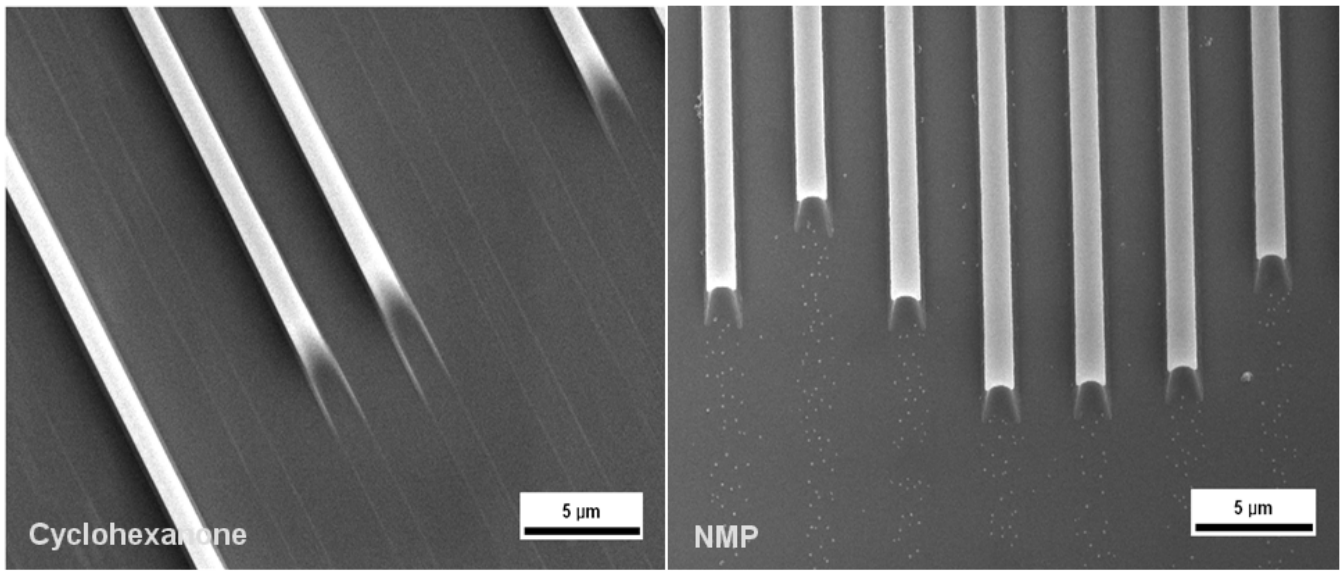

Figure S4. SEM images of the ends of the PDO 3 lines from cyclohexanone (left panel) and NMP (right panel): The PDO 3 solution of NMP exhibits higher advancing contact angle compared to that of cyclohexanone due to the lower interfacial free energy.

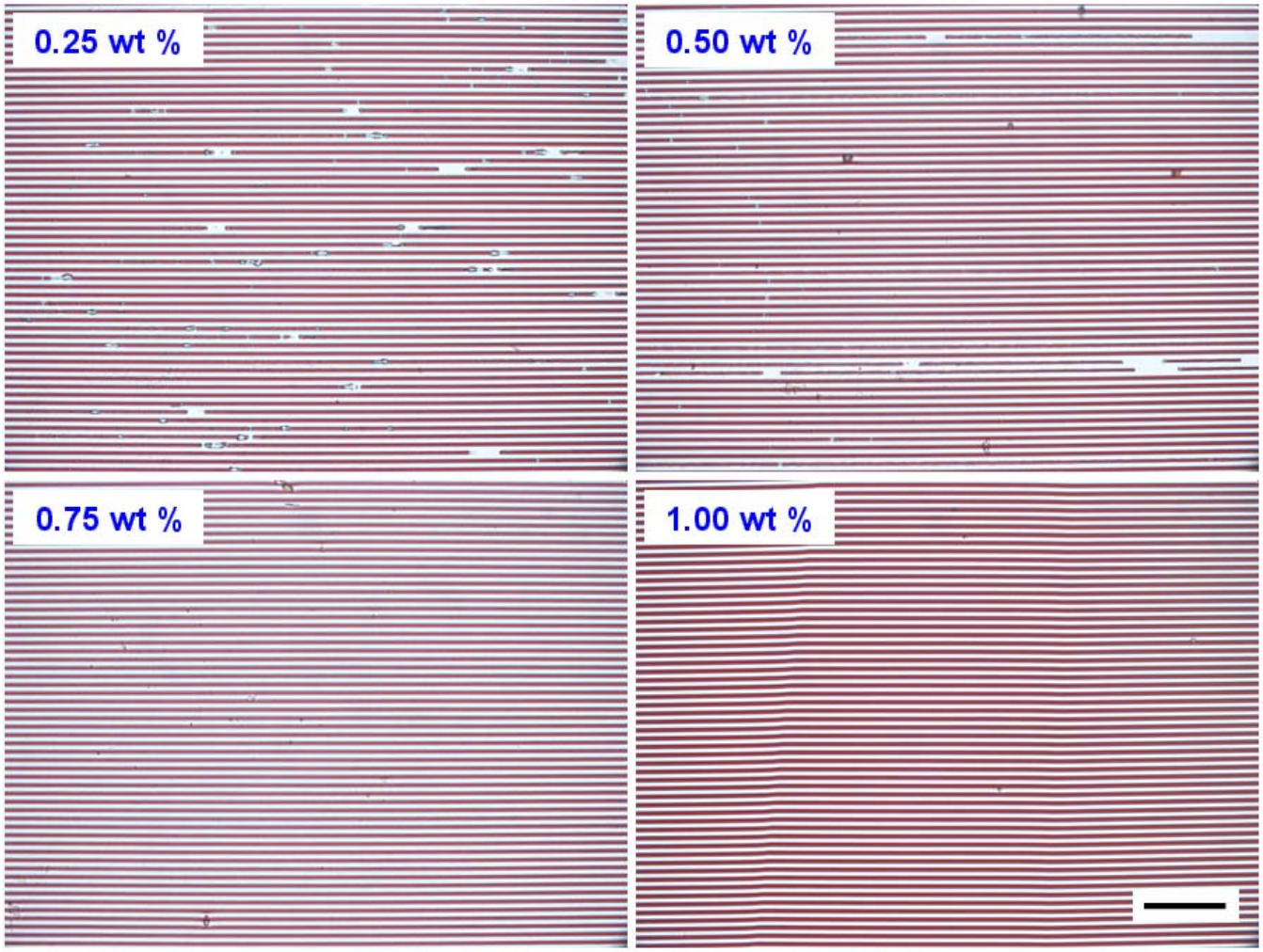

Figure S5. OM images of the fabricated PDO 3 line arrays by MIMIC with NMP versus the concentration of the PDO 3 solutions: The scale bar is 40 μm.

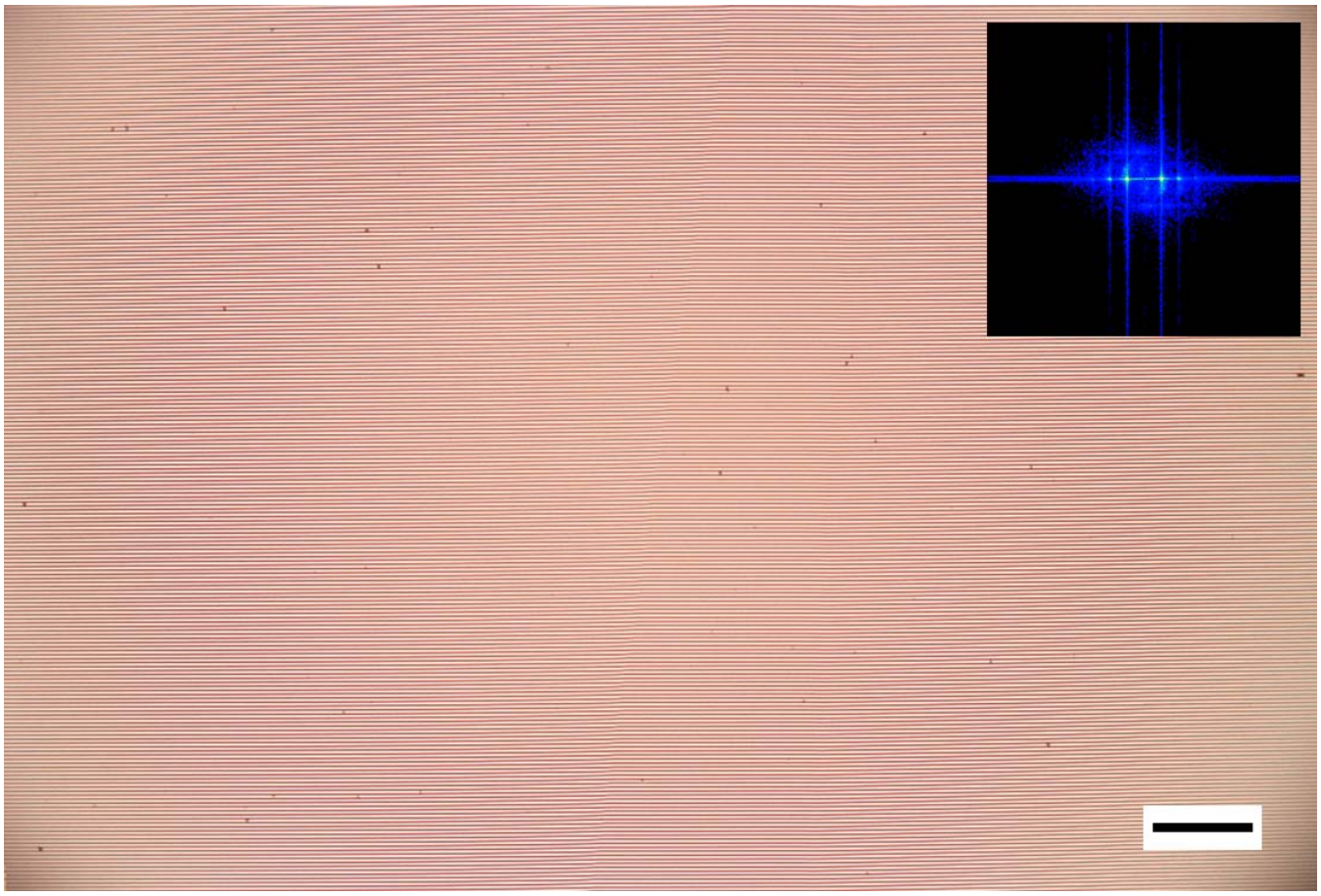

Figure S6. Low-magnification OM image of the fabricated PDO 3 line arrays (1.00 wt% PDO 3 solutions in NMP). In the inset, Fourier transform (FT) of the corresponding OM image is shown. PDO 3 lines arrays are uniformly fabricated over a large area (~mm^2) as evidenced from the moiré fringe of OM image and FT. The scale bar is 100 μm.

3. Optical setup for one beam and interference pattern irradiation

We used a conventional transmittance holographic optical setup for the beam irradiation experiment as described in Figure S7. In the single-beam irradiation experiment, one of the beams was blocked, and the sample stage was rotated to irradiate the sample at a normal angle. The intensity and polarization of the beams were controlled using a neutral density (ND) filter and a half-wave (HW) plate, respectively. The irradiation time was precisely controlled through the use of an electronic shutter.

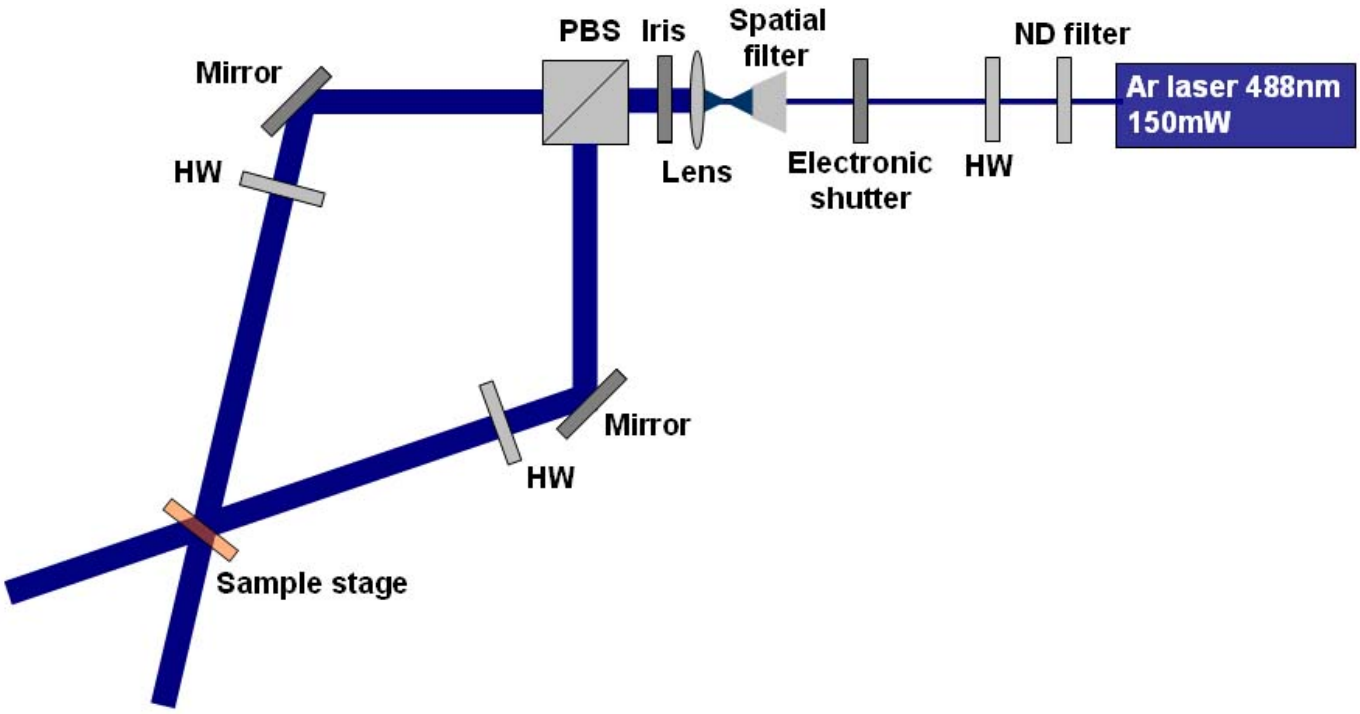

Figure S7. Schematic illustration of the optical setup of the single-beam and interference pattern irradiation: ND filter – Neutral density filter; HW – Half-waveplate; PBS – Polarizing beam splitter.

4. PDO 3 lines after irradiation by one beam with polarization perpendicular to the grating vector of line arrays (*p*-polarization)

As shown in Figure S8, the irradiation of light with *p*-polarization did not give rise to directional photofluidization (lateral expansion). However, interestingly, we found that the line-edge roughness was significantly reduced. This reduced line-edge roughness can be attributed to the fact that photofluidization of azopolymer works under the surface energy. The fluid behavior of azopolymer preferentially minimize the surface energy similar to that of the thermal flow of a polymer resist with a low-glass-transition temperature.[6]

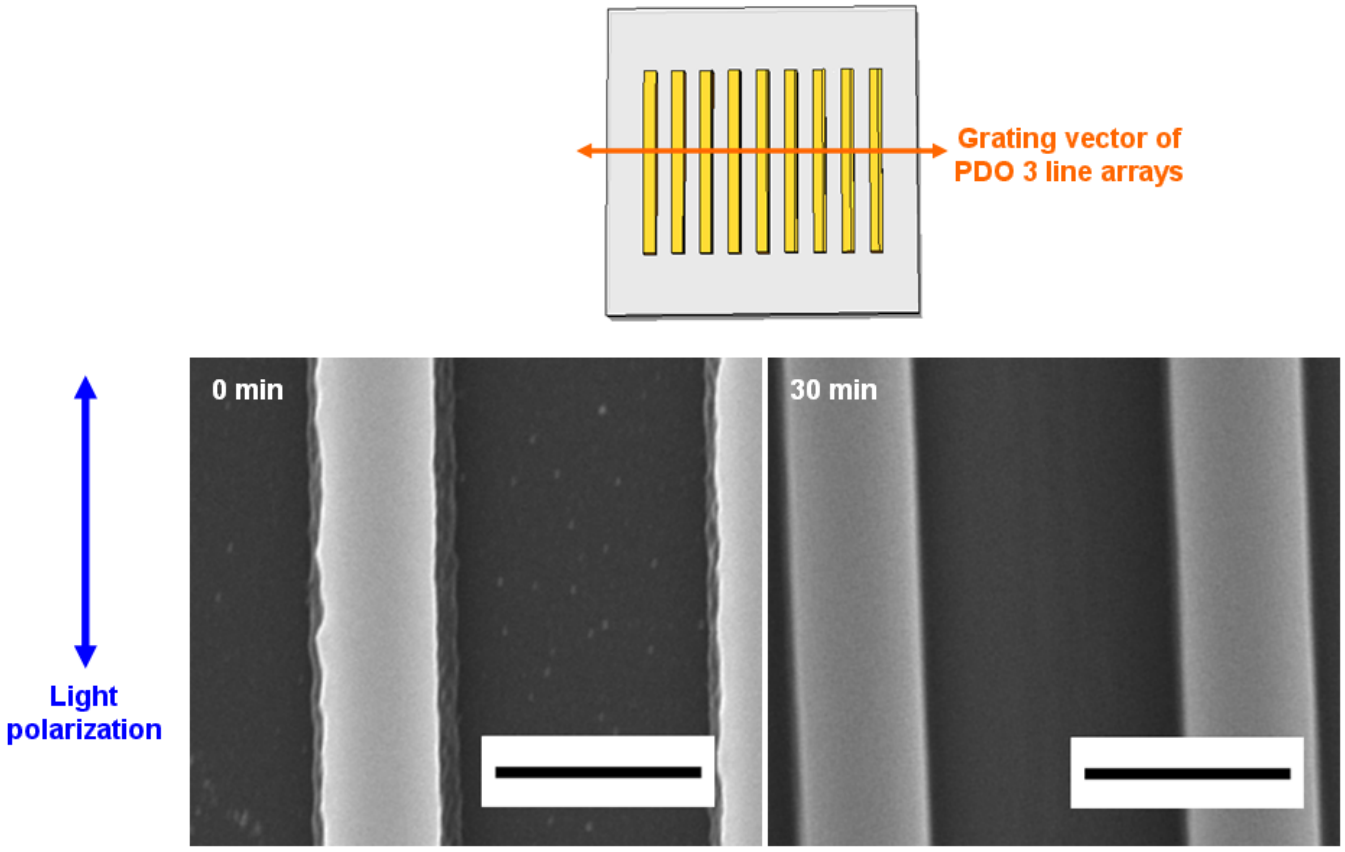

Figure S8. SEM images of photo-reconfigured PDO 3 lines by single-beam irradiation with *p*-polarization (perpendicular to the grating vector of PDO 3 line arrays): The scale bars are 2 μm.

5. Intensity profile of interference pattern along grating vector

The formation of a hole having a streamline is attributed to the unique characteristic sinusoidal intensity profile of the interference light pattern, as shown in Figure S9; the length of the arrow indicates the intensity of the light.

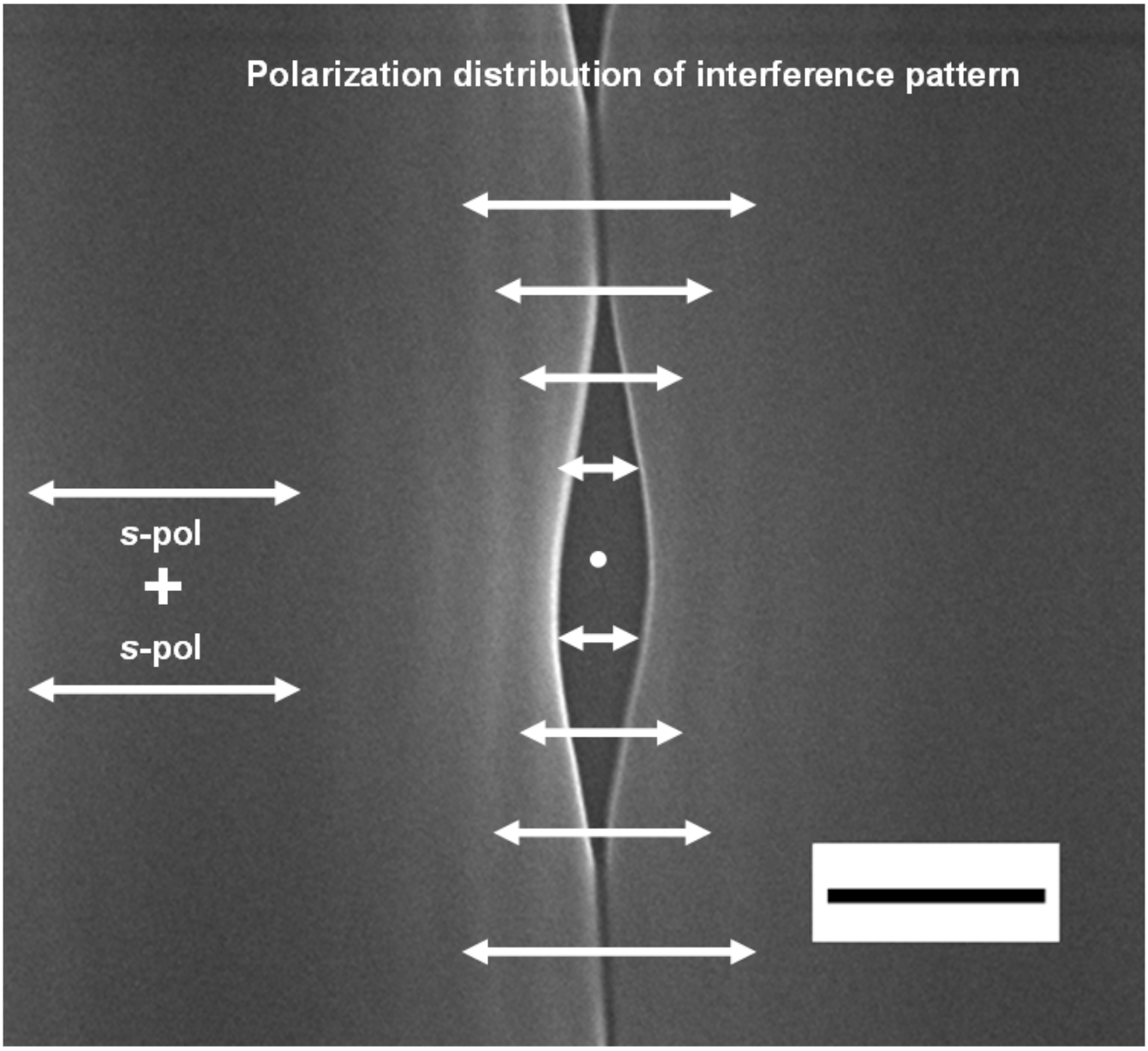

Figure S9. Schematic illustration of the polarization distribution along the interference pattern: Scale bars are 1 μm.

6. Experimental setup for measuring the optical scattering of gold ellipsoids

Transverse mode of optical scattering

The experimental setup for measuring the optical scattering (transverse mode of surface plasmon, visible to near-infrared) of gold ellipsoids (see Figures S10) is based on that reported by Whitesides et al.[7] The micro-reflectance system was built on a standard optical microscope (OM, Olympus, BX51): a thermo-electrically cooled CCD detector (DV401A-BC, iDUS CCD detector, Andor technology) was equipped, as described in Figure S11. An unpolarized, spatially filtered 100 W halogen light source (Fiber Illuminator OSL1) was irradiated at an incident angle of 60° (dark-field illumination); this slant irradiation can maximize the optical scattering of the gold ellipsoids.[8] The scattered light was collected by a 50× microscopic objective lens (Mitutoyo NIR M plan APO, numerical aperture (NA) = 0.42), and was then filtered by an analyzer parallel to the short axis of the gold ellipsoid to select the transverse mode of the surface plasmon resonance (transverse to the long axis of the gold ellipsoid). Finally, the selected light arrived at the spectrometer.

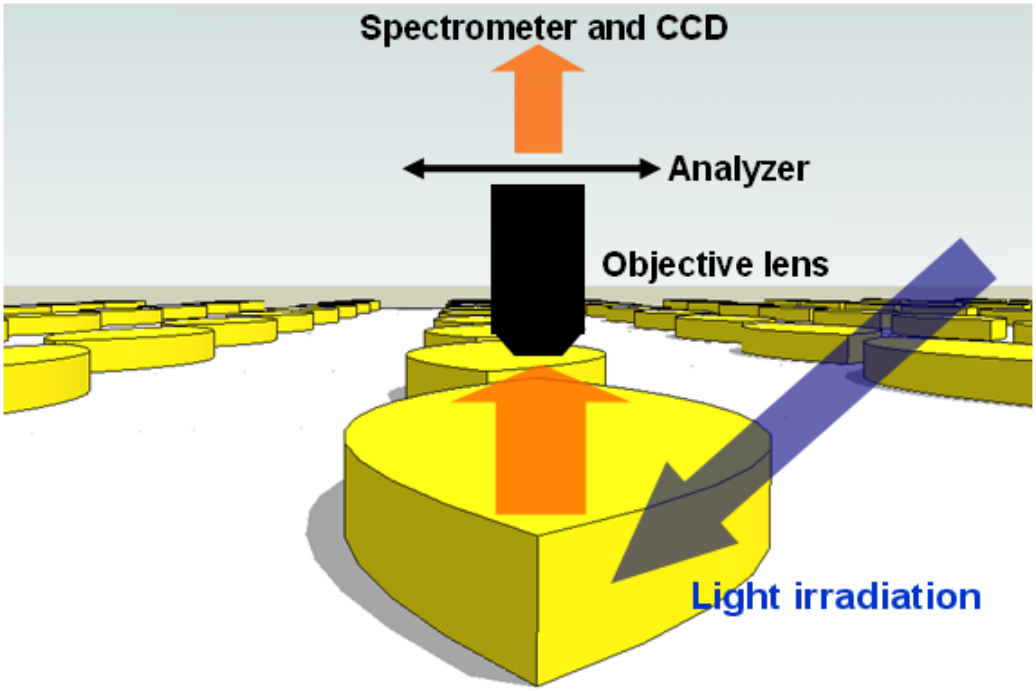

Figure S10. Schematic illustration of the experimental setup used to measure the optical scattering of gold ellipsoids: The incident angle of light was 60° with respect to the normal direction of the substrate.

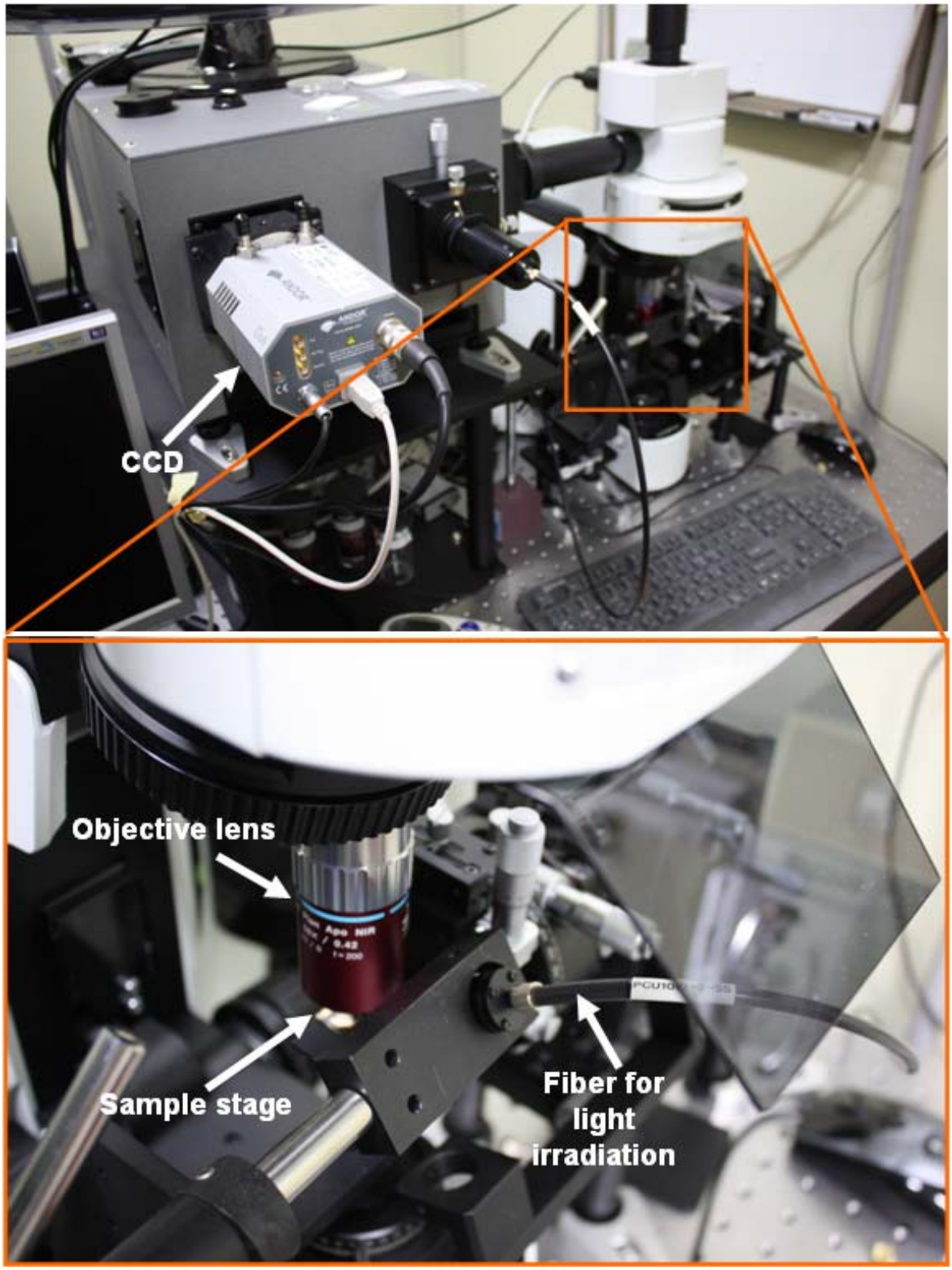

Figure S11. Digital photographs of the experimental setup used to measure the optical scattering of gold ellipsoids

Longitudinal mode of optical scattering

The optical scatterings (longitudinal mode of surface plasmon, infrared) of the gold ellipsoids were characterized by Fourier-transform infrared spectroscopy (Bruker IFS 66 V/S) combined with an IR microscope (Hyperion 3000, Nikon).

7. Finite-Difference Time-Domain (FDTD) simulation: Surface plasmons of gold ellipsoids

A numerical simulation was conducted using the finite-difference time-domain method.[9] In this simulation, Yee's discretization scheme was utilized.[10] The lateral sizes of the computational domain were set equal to the periods of the fabricated sample (two-beam irradiation of 90 min) and a periodic boundary condition was adopted.[9] Perfectly matched layers[11] terminate the domain in the vertical direction at 2 μm. The computational domain is discretized in 2 to 4 nm steps. Mirror symmetries are exploited to reduce the computation by two- or four-fold when possible.

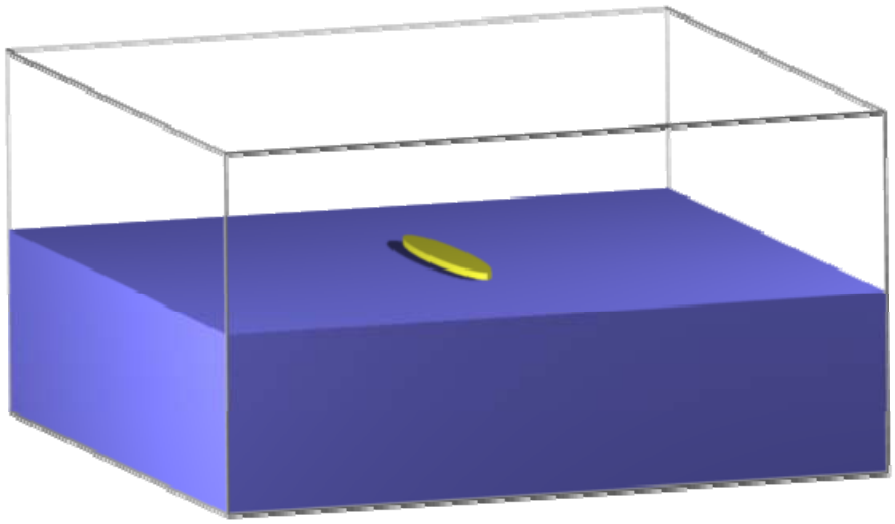

Figure S12. Computational domain for the time domain simulation: The blue block indicates the quartz substrate, the yellow ellipsoid the gold nanostructure, and the gray lines the domain boundaries.

REFERENCES.

(1) Wang, W. *et al.* Epoxy-based nonlinear optical polymers from post azo coupling reaction. *Macromolecules* **30**, 219—225 (1997).

(2) Kim, M.-J., Yoo, S.-J. & Kim, D.-Y. A Supramolecular Chiroptical Switch Using an Amorphous Azobenzene Polymer. *Adv. Funct. Mater.* **16**, 2089—2094 (2006).

(3) Levenson, M. D. Wavefront engineering for photolithography: New optical techniques based on the application of fundamental physical principles to photomask design may bring about a revolution in the patterning of integrated circuits. *Physics Today* **46**, 28—36 (1993).

(4) Kim, E., Xia, Y. & Whitesides, G. M. Micromolding in capillaries: Applications in materials science. *J. Am. Chem. Soc.* **118**, 5722—5731 (1996).

(5) Kim, E. & Whitesides, G. M. Imbibition and flow of wetting liquids in noncircular capillaries. *J. Phys. Chem. B* **101**, 855—863 (1997).

(6) Yu, Z., Chen, L., Wu, W., Ge, H. & Chou, S. Y. Fabrication of nanoscale gratings with reduced line edge roughness using nanoimprint lithography. *J. Vac. Sci. Technol. B* **21**, 2089—2092 (2003).

(7) Xu, Q., Bao, J., Capasso, F. & Whitesides, G. M. Surface plasmon resonances of free-standing gold nanowires fabricated by nanoskiving. *Angew. Chem. Int. Ed.* **45**, 3631—3635 (2006).

(8) Schultz, S., Smith, D. R., Mock, J. J. & Schultz, D. A. Single-target molecule detection with nonbleaching multicolor optical immunolabels. *Proc. Natl. Acad. Sci. USA* **97**, 996—1001 (2000).

(9) Fan, S., Villeneuve, P. R. & Joannopoulos, J. D. Large omnidirectional band gaps in metallodielectric photonic crystals. *Phys. Rev. B* **54**, 11245—111251 (1996).

(10) Yee, K. S. Numerical solution of initial boundary value problems involving Maxwell's equations in isotropic media. *IEEE Trans. Antennas Propagat.* **AP-14**, 302—307 (1996).

(11) Berenger, J. A perfectly matched layer for the absorption of electromagnetic waves. *J. Comput. Phy.* **114**, 185—200 (1994).